

ACKNOWLEDGMENTS

We wish to thank Dr. R. Clive Field for help during the first stages of the experiment and Dr.

William R. Holley for many helpful discussions. Michael Barnes and John P. Wilson assisted thoughtfully during the data analysis and we gratefully acknowledge their participation.

*Work done under the auspices of the United States Atomic Energy Commission.

†Present address: Enrico Fermi Institute of Physics, University of Chicago, Chicago, Illinois 60637.

¹E. S. Shrum and K. O. H. Ziok, *Phys. Lett.* **37B**, 115 (1971).

²P. S. L. Booth, R. G. Johnson, E. G. H. Williams, and J. R. Wormald, *Phys. Lett.* **26B**, 39 (1967).

³Karl-Erik Bergkvist, CERN Report No. CERN 69-7, 1969 (unpublished), p. 91.

⁴Alan R. Clark, T. Elioff, R. C. Field, H. J. Frisch, Rolland P. Johnson, Leroy T. Kerth, and W. A. Wenzel, *Phys. Rev. Lett.* **26**, 1667 (1971).

⁵H. J. Frisch, thesis, UCRL Report No. UCRL-20264, 1971 (unpublished).

⁶E. S. Ginsberg, *Phys. Rev.* **171**, 1675 (1968). Dr. Ginsberg kindly gave us copies of programs to calculate the relevant radiative corrections.

⁷D. S. Ayres, A. M. Cormack, A. J. Greenberg, R. W. Kenney, D. O. Caldwell, V. B. Elings, W. P. Hesse, and R. J. Morrison, *Phys. Rev. D* **3**, 1051 (1971). Using the $V-A$ theory to calculate the dependence of the transition probability $\Gamma(\pi^\pm \rightarrow \mu^\pm \nu)$ on neutrino mass, the 90% C.L. limit on the difference between the muon neutrino and its antiparticle is found for that experiment to be ~ 4 MeV.

PHYSICAL REVIEW D

VOLUME 9, NUMBER 3

1 FEBRUARY 1974

Wide-gap spark-chamber study of $K_L^0 \rightarrow \pi + e + \nu$ decay*

L. Wang, † R. C. Smith, ‡ M. C. Whatley, § and G. T. Zorn
University of Maryland, College Park, Maryland 20742

J. Hornbostel ||

Brookhaven National Laboratory, Upton, New York 11973

(Received 16 February 1973)

A wide-gap spark chamber operated in a magnetic field has been used to measure the energy dependence of the form factor $f_+(q^2)$ in $K_L^0 \rightarrow \pi + e + \nu$ decay. Decays of K_L^0 mesons in vacuum were detected in the -30° neutral beam of the AGS at Brookhaven National Laboratory. K_{e3}^0 decays were identified by electromagnetic showers produced in a lead radiator plate between the two 12-inch gaps of the chamber. The linear parameter λ_+ in the form factor $f_+(q^2)$ was determined to be 0.040 ± 0.012 , where the error includes uncertainties in the corrections for systematic effects. A study of these systematic effects and the resulting errors is presented.

I. INTRODUCTION

The predictions of the $V-A$ theory are very successful for processes that involve nonstrange particles.^{1,2} It is natural to try to apply the same theoretical considerations to weak processes involving strange particles.² In particular, the three-body leptonic decays of K mesons have been the subject of a number of studies.

The transition matrix element for K_{l3} decay is usually written in the form³

$$M = \frac{G}{\sqrt{2}} \sin\theta [\bar{u}_l \gamma_\alpha (1 + \gamma_5) u_\nu] \langle \pi | V_\alpha^\dagger | K \rangle,$$

where G is the Fermi coupling constant and θ is

the Cabibbo angle given by the Cabibbo theory of semileptonic weak interactions. The pion and the K meson are taken to have the same intrinsic parity, and a pure vector interaction is assumed in the framework of $V-A$ theory. The last factor describes the hadron interaction in the decay.

The constraint of four-momentum conservation reduces the number of independent four-momenta in the interaction to two, and the matrix element can be written in terms of the four-momenta:

$$q_\alpha = (p_K - p_\pi)_\alpha, \\ Q_\alpha = (p_K + p_\pi)_\alpha,$$

where $\alpha = 1, 2, 3,$ or 4 . The hadronic part of M

is written in the form

$$\langle \pi | V_\alpha^\dagger | K \rangle = \frac{1}{2(2E_K \times 2E_\pi)^{1/2}} \times [f_+(q^2)Q_\alpha + f_-(q^2)q_\alpha],$$

where, from the requirement of Lorentz invariance, the form factors f_+ and f_- are functions of q^2 only. The quantity q^2 , which is the square of the four-momentum transfer, can be expressed in terms of the pion total energy in the K rest frame, E_π^* , as

$$q^2 = (p_K - p_\pi)^2 = m_K^2 + m_\pi^2 - 2m_KE_\pi^*.$$

Thus the transition probability is

$$\begin{aligned} \frac{d^2N}{dE_\pi^* dE_\nu^*} \propto & [m_K(2E_\nu^*E_\pi^* - m_KE_\nu') \\ & + m_l^2(\frac{1}{4}E_\nu' - E_\nu^*)]f_+^2(q^2) \\ & + m_l^2(E_\nu^* - \frac{1}{2}E_\nu')f_+(q^2)f_-(q^2) \\ & + m_l^2(\frac{1}{4}E_\nu')f_-^2(q^2), \end{aligned}$$

where

$$E_\nu' = E_{\pi \max}^* - E_\pi^* = \frac{m_K^2 + m_\pi^2 - m_l^2}{2m_K} - E_\pi^*.$$

The form factors $f_+(q^2)$ and $f_-(q^2)$ are analytic functions of q^2 , except for a cut given by $(-q^2) > (m_K + m_\pi)^2$. In the physical region it is reasonable to assume that they are slowly varying functions. They are usually approximated by expressions which are linear in q^2 , namely,¹⁻³

$$\begin{aligned} f_+(q^2) &= f_+(0)(1 + \lambda_+ q^2/m_\pi^2), \\ f_-(q^2) &= f_-(0)(1 + \lambda_- q^2/m_\pi^2). \end{aligned}$$

The ratio $[f_-(0)/f_+(0)]$ is usually referred to as $\xi(0)$.

In K_{e3}^0 decay, the effect of the f_- form factor is small due to the small mass m_e , and as a result both λ_- and $\xi(0)$ are inaccessible to measurement. In $K_{\mu 3}$ decay, λ_+ , λ_- , and $\xi(0)$ can all be measured; however, the correlation between them makes their simultaneous determination more subject to error.³ If muon-electron universality is assumed, the form factors for $K_{\mu 3}$ and K_{e3} are identical. Thus the single-parameter analysis of K_{e3} decay not only can result in a more certain value for λ_+ , but can be used to reduce the three-parameter analysis of $K_{\mu 3}$ decay into a two-parameter analysis, thereby giving more precise values for λ_- and $\xi(0)$. In addition it is noted that measurements of λ_+ in K_{e3}^0 and K_{e3}^+ decay can be used to test the $\Delta I = \frac{1}{2}$ rule, which predicts equal λ_+ values.

In this paper an experimental study of the K_{e3}^0 decay mode is presented, in which the energy depen-

dence of the $f_+(q^2)$ form factor and thereby λ_+ was measured. Precautions were taken in the handling of possible systematic biases and the sensitivities to systematic effects were evaluated. The paper is divided into five sections. The experimental apparatus and the event selection are described in Sec. II. The analysis of the data and the determination of the λ_+ parameter are presented in Sec. III. Systematic effects and resulting errors are discussed in Sec. IV. Finally, the paper is concluded in Sec. V with a discussion of results.

II. EXPERIMENTAL ARRANGEMENT

A. The beam

The source of K_L^0 mesons used in this experiment was a neutral beam coming from an internal beryllium target in the alternating-gradient proton synchrotron (AGS) located at Brookhaven National Laboratory. A sketch of the beam layout is shown in Fig. 1. The collimator system and a sweeping magnet selected neutral secondary particles at 30° to the direction of proton beam. To reduce the γ -ray flux in the beam, four inches of lead were placed upstream of the first collimator. The center of the beam-defining collimator was 25 ft from the target and the decay region was 70 ft from the target.

During this experiment, the AGS was operated at 28.5 GeV with 0.5×10^{12} to 2×10^{12} accelerated protons per beam pulse. The pulse duration was 0.5 sec and the repetition rate was 0.4/sec.

The K_L^0 momentum spectrum was experimentally determined.⁴ The observed spectrum peaks at $p_K = 0.5$ GeV/c and falls to 10% of its peak value at $p_K \cong 2.0$ GeV/c.

B. The detector

The detector was a triggered wide-gap spark chamber which had a momentum resolution of ± 20 MeV/c at 450 MeV/c and covered a forward solid angle of ~ 0.5 sr. This detector was appropriate for the study of K_{e3}^0 decays in the K_L^0 beam described, as the detection efficiency had a small q^2 dependence [see Fig. 15(b)] and as the center-of-mass energy resolution was $\sim \pm 10$ MeV/c².

A drawing of the detector system is shown in Fig. 2. The entire system was placed inside a magnet. The magnet, which formerly had been used as a bubble-chamber magnet, had a 22-in. gap and 30-in. pole pieces. One of the pole pieces consisted of a hollow tube through which the chamber was photographed. Prior to the experiment, the field of this magnet was mapped at the operating current.⁵ The central field was 10.4 kG and fell off to 8.5 kG at a radial distance of 13.5 in.

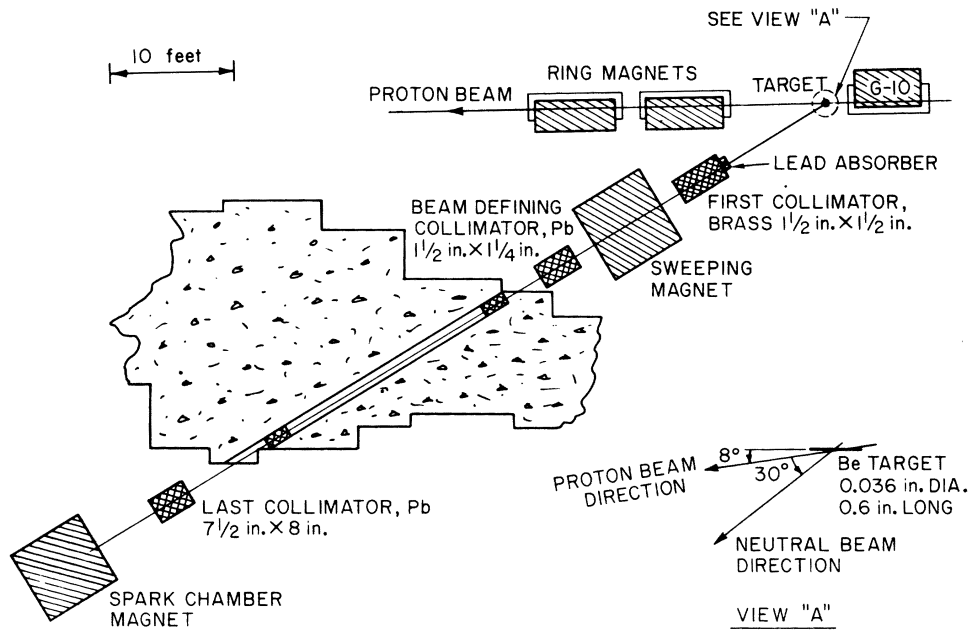


FIG. 1. Beam layout.

The magnet current was maintained constant to within $\pm 0.05\%$. The polarity of the magnet was systematically reversed during film changes to permit charge asymmetry studies of the K_{73}^0 decay mode.

A vacuum box (not shown in Fig. 2) contained

counters S_1 , S_2 , and A . The windows of the vacuum box were made from thin aluminum sheets ($\sim \frac{1}{32}$ in. thick). Counters S_1 and S_2 consisted of twelve individually-wrapped plastic scintillators of dimensions $1 \times \frac{1}{8} \times 10$ in.³ As shown schematically in

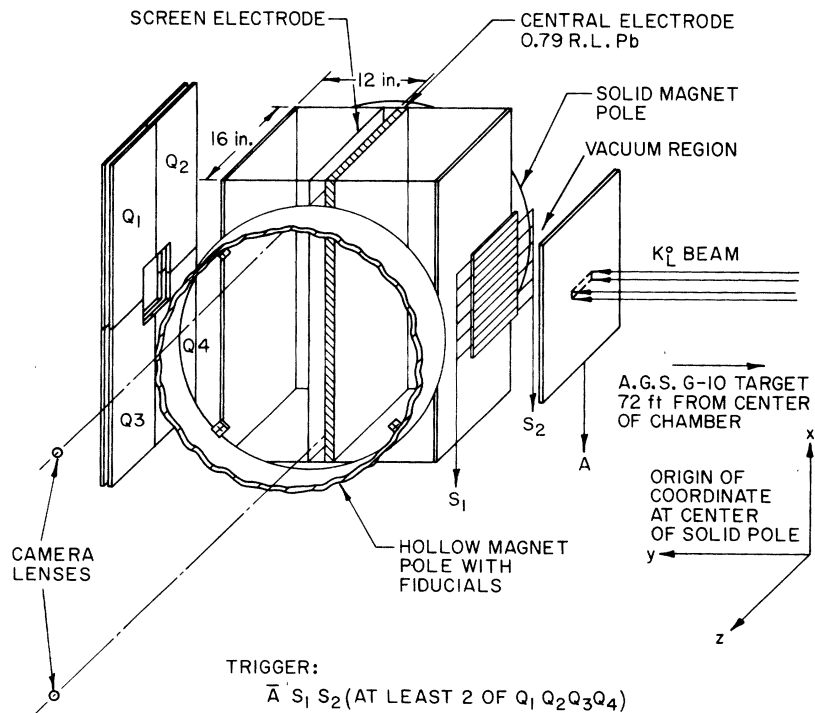


FIG. 2. Scale drawing of detector.

Fig. 2, the light from these scintillators was alternately directed with light pipes to one of two photomultiplier tubes. Four pairs of scintillation counters, Q1, Q2, Q3, and Q4, were used downstream from the spark chamber. All counters were tested and were found to be more than 99% efficient for minimum-ionizing particles at normal incidence over their entire sensitive areas.

The wide-gap spark chamber had two 12-in. gaps and inside dimensions of 16 in. by 30 in. The plates of the chamber were 0.001 in. aluminum foil stretched and epoxied to narrow aluminum frames. Mylar sheets 0.005 in. thick were used as outside windows over these frames to contain the gas mixture. The frame of the center plate was 1 in. thick and was so constructed that a plate of high- Z material (or radiator) could be inserted. A radiator sandwich (0.150 in. of lead and 0.063 in. of brass) with a total of 0.79 radiation lengths was used. This radiator served to identify electrons by the showers they produced in it. The radiator also served to convert γ rays which were used to tag the $K_L^0 \rightarrow \pi^+ + \pi^- + \pi^0$ decay mode. The results on $K_{\pi_3}^0$ decay mode were reported previously.⁸

The downstream chamber had an additional screen electrode 1.75 in. from the center plate. (See Fig. 2.) This screen electrode enhanced the chamber efficiency for detecting low-energy electrons of the shower. Electrons or positrons with $p > 20$ MeV/ c leaving the radiator at an angle of $> 45^\circ$ were seen with high efficiency ($\approx 95\%$).

The chamber was operated at ~ 1 in. of water above atmospheric pressure, with a gas mixture of 90% neon and 10% helium with 2.2 Torr of ethanol vapor. The gas was recirculated through a series of filters including an activated charcoal filter at liquid-nitrogen temperature. The ethanol vapor was added to the gas as it returned to the chamber. The high-voltage pulse was provided by a pressurized 12-stage Marx generator with a nominal capacitance of 7800 pF per stage. The risetime of the high-voltage pulse produced was < 5 nsec. In order to match the effective risetime of the whole chamber assembly (≈ 50 nsec), a resistor was inserted in series with the chamber. The voltage maximum which appeared on the chamber was ~ 280 kV. A resistor-capacitor network, powering equally-spaced wires surrounding the chamber, distributed this pulsed potential uniformly across the two gaps of the chamber. The chamber was operated in an aluminum rf enclosure in which Freon-12 was introduced to suppress sparking. A detailed description of the high-voltage system and the characteristics of the chamber are given elsewhere.⁷

The chamber was photographed by two cameras with optical axes parallel to the central magnetic-

field direction. The stereo angle at the center of the chamber was about 22° and the demagnification was $\frac{1}{37}$. The film used was 35-mm Kodak type SO-340. Photographs were taken through a coarse screen ($\frac{1}{4}$ -in. wire spacing) which replaced a cut-out section of the rf enclosure and through a 1.5-in. thick acrylic plate, which was used for high-voltage insulation of the chamber. In addition, an array of gray filters was mounted between two $\frac{1}{4}$ -in. acrylic plates and placed between the cameras and the chamber. This array consisted of 96 quarter-inch-wide vertical gray strips in a repeated pattern with transmission percentages of 100%, 30%, 10%, and 3%. The purpose of these filters was to enable photography of the central core of each track at six to nine points along its length in each gap, even with large variation in track brightness.⁸ Also appearing in each photograph were four fiducial marks and a data panel giving information on each event.

Figure 3 is a photograph of a $K_L^0 \rightarrow \pi^- + e^+ + \nu$ event taken under normal conditions. The lower track was produced by a pion. The upper track was produced by a positron, which in turn produced a shower in the center plate. There were two elec-

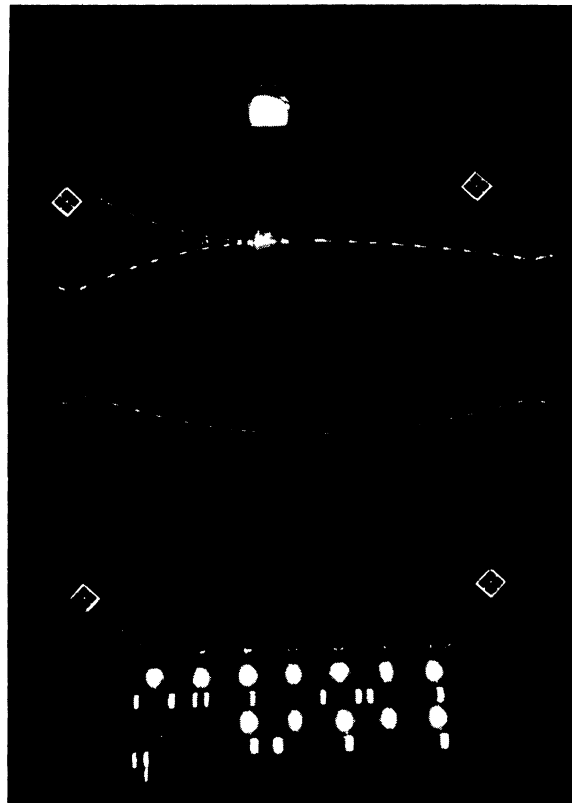


FIG. 3. Photograph of K_L^0 decay.

trons and two positrons in the shower. One of these positrons at low momentum made a 180° arc and reentered the center electrode near the bottom of the chamber. The effectiveness of the gray filters and of the additional screen electrode can be readily seen in this photograph.

C. Trigger circuitry

Figure 4 shows a schematic diagram of the trigger logic. The requirement of this logic was that counter *A* not count but that S_1 , S_2 , and at least two of the four pairs Q_1 , Q_2 , Q_3 , and Q_4 , count in coincidence. This ensured the detection of neutral particles decaying within the vacuum into two (or more) charged particles that did traverse the chamber. Spurious tracks were seldom seen with V events in the wide-gap chambers, indicating a spurious-track rate much less than $\sim 10^5/\text{sec}$, which is the reciprocal of the spark-chamber memory time.

The total time delay between the passage of a particle and the arrival of the high-voltage pulse on the chamber was 240 nsec, 75 nsec of which was associated with the amplifier, spark-gap, and Marx-generator circuitry. As the track distortion was found to increase with increasing delay, a separate timing circuit was used during the runs to check that the total delay did not exceed ~ 300 nsec. A special data light was lit and photographed for events with delays more than 300 nsec. These events ($\sim 2\%$ of all events) were not included in the analysis.

D. Data collection

Two-view pictures of each event were recorded on 35-mm film. Special runs were made at the beginning of each roll to monitor and check the efficiency and the accuracy of track location for the

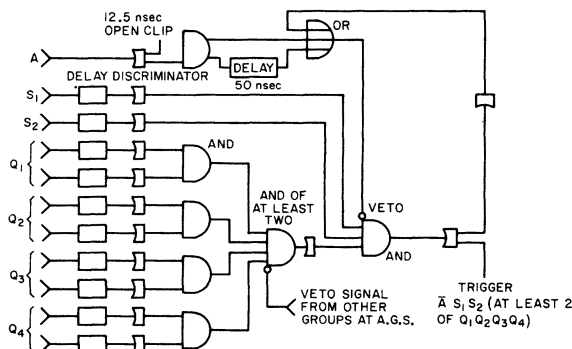


FIG. 4. Schematic drawing of trigger logic.

wide-gap chamber. Included in these were runs with no magnetic field and runs in which a 4-in. copper absorber, acting as a K_S^0 regenerator, was placed 2.25 in. upstream from the anticounter *A*. 10% of all pictures taken were special runs.

The photographs taken during the experiment were projected on tables for scanning and, if selected, were measured immediately using the image-plane digitizers.⁹ The projection was at $\sim \frac{2}{3}$ of the actual size. A total of 140 000 frames taken under normal conditions was scanned and 17 000 $K_{\pi^3}^0$ and $K_{e^3}^0$ candidates were measured. Another 5000 frames of the special runs also were scanned and measured.

For standard runs, $K_{e^3}^0$ and $K_{\pi^3}^0$ candidates were selected by electron-shower and converted γ -ray signatures, respectively. In both cases, the first criterion was that in the upstream chamber gap, there be two (and only two) tracks of different charge. For $K_{e^3}^0$ candidates, it was further required that one of these upstream tracks be associated with two or more tracks in the downstream gap, or be associated with one track of opposite charge. (These charge-exchange-type events were seen in 5% of $K_{e^3}^0$ events.) For $K_{\pi^3}^0$ candidates, the second criterion was that there be at least one downstream track not associated with an upstream track, giving the appearance of a track from a γ -ray conversion. The results of the scanning can be summarized as follows:

(i) 4% of all frames satisfied the criteria for $K_{e^3}^0$ decay.

(ii) 9% satisfied the criteria for $K_{\pi^3}^0$ decay.

(iii) 37% were V events that appeared without an associated e - m shower or a converted γ ray.

The above numbers are consistent with the Monte Carlo calculation, which predicts that the observed ratios between (a) $K_{e^3}^0$ events with an electromagnetic shower, (b) $K_{\pi^3}^0$ events with a converted γ ray, (c) $K_{e^3}^0$ events without a shower, (d) $K_{\pi^3}^0$ events without a converted γ ray, and (e) detected $K_{\mu^3}^0$ events should be 1:2:4:2:3.

(iv) $<0.05\%$ of all frames had events with two track-associated showers and events with both a converted γ ray and a track-associated shower. These can be explained as resulting from the nuclear interaction of a secondary pion in the central radiator.

(v) 15% of all frames had two tracks of the same charge in the upstream gap. Since they were found to come exclusively from the windows of the vacuum enclosure and the counters S_1 , S_2 , and *A* they were presumably produced in the nuclear interactions of beam particles in these materials.

(vi) 35% of all frames had only one track in the upstream gap or were V events with random surface breakdown. These breakdowns were found to

be uncorrelated with track position.

One third of the scanned frames, i.e., 50 000 frames, including all those scanned during the training period of the scanners, were rescanned. Based on this rescan the efficiency for a single scan was found to be 96%. Of the 4% missed, about half contained a very wide dark track or a track which hit the wall of the chamber and was mistaken as a chamber breakdown. About a quarter of the events missed had one track whose charge changed sign at the radiator; such events were normally classified as K_{e3}^0 events as described in the previous paragraph.

Events were measured as they were found. Six to nine points were measured on each track in each view. These points were chosen in the segments where the gray filters had reduced the track width to about 1 mm in space. The downstream gap of the chamber was divided into two parts by the screen electrode (see Fig. 2). Tracks that were registered in both parts were measured in the wider gap. Tracks of all visible shower secondaries were measured.

E. Reconstruction and selection of events

The measurements on events were corrected for optical distortions produced both in picture taking and in projection on measurement tables. Tracks were reconstructed in three-dimensional space using a computer program TVGP¹⁰ written for track reconstruction in bubble chambers. The Coulomb scattering and ionization energy loss features in TVGP were excluded. The optical constants used in TVGP were calculated by another computer program FIDCON,¹¹ also written for use in bubble-chamber experiments. Tracks that were reconstructed by TVGP and their associated error matrices were extrapolated into the vacuum decay region. The point of closest approach between the two tracks was taken as the decay vertex. Laboratory quantities at this vertex then were used for the zero-constraint kinematic reconstruction of the event in the kaon center-of-mass system. It was in this calculation that a twofold ambiguity resulted in the calculated value for the kaon momentum and, of course, also for center-of-mass quantities.

A total of 4364 events were measured as K_{e3}^0 candidates. To remove background events and those which might produce systematic biases, the following criteria were used to select the final sample:

(a) Only those events with a distance of closest approach for tracks, ρ , of <0.7 cm were selected, thereby eliminating events with large scattering angles or large measurement errors. Figure 5 shows the ρ distribution and the limiting value that

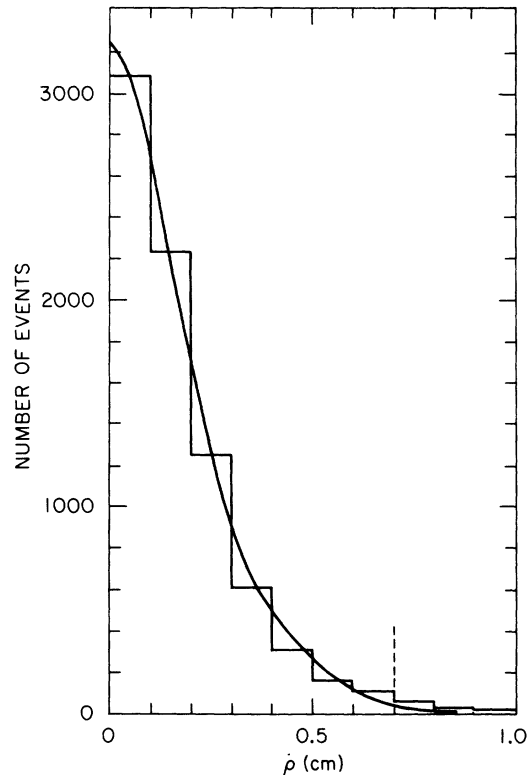


FIG. 5. Histogram of the distance of closest approach at the vertex, ρ (in cm) for $K_{\pi 3}^0$ and $K_{e 3}^0$ events. The smooth curve is the Monte Carlo prediction. $\chi^2=8$ for 6 degrees of freedom. Dashed line indicates limit applied in selection of data and in the χ^2 calculation.

was used. (91 events were rejected in applying this criterion.)

(b) The projected distributions of vertex positions along x , z , and y inside the vacuum box are shown in Figs. 6, 7, and 8, respectively. The effect of the scattering of K_L^0 mesons by the lead γ -ray absorber and by the beam-defining collimator walls results in long flat tails on the x and z distributions. To restrict the number of these scatterings in our sample, events were included only if their vertices occurred in the intervals $-2.5 < x < 2.5$ cm and $18.5 < z < 35.5$ cm. The effect of events produced by scattered K_L^0 mesons still remaining in the sample was estimated and corrections for it were made. [See Sec. III A(b).] To eliminate background events resulting from nuclear interactions in the A and S counters and the aluminum windows of the vacuum box, y was required to be within the interval $-66.4 < y < -43.8$ cm. The vacuum region between counters A and S lay between $y = -67.1$ cm and $y = -43.1$ cm. (472 events were rejected.)

(c) The upstream tracks of an event were required to traverse the radiator inside a central

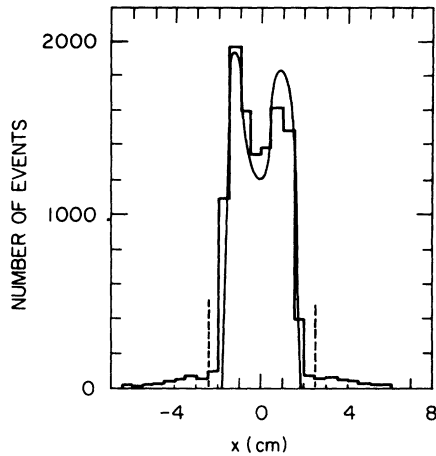


FIG. 6. Distribution of event vertices; projection along x (cm). Smooth curve represents the Monte Carlo prediction. $\chi^2=34$ for 9 degrees of freedom. Dashed lines indicate limits applied in selection of data and in the χ^2 calculation.

area of 35×50 cm² so that any shower produced would be visible in the 40×75 cm² downstream gap and that no tracks would traverse the walls of the spark chamber. The distributions of the traversal points for electrons and for pions in K_{e3}^0 decay are shown in Figs. 9 and 10, respectively. At the radiator the tracks also were required to be separated by a distance of 2 cm so that the shower could be unambiguously associated with only one of the tracks. At the radiator plane, the shower tracks were required to extrapolate to within 1 cm

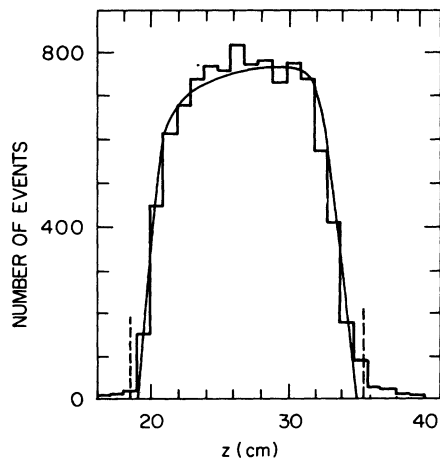


FIG. 7. Distribution of event vertices; projection along z (cm). Smooth curve represents the Monte Carlo prediction. $\chi^2=14$ for 16 degrees of freedom. Dashed lines indicate limits applied in selection of data and in the χ^2 calculation.

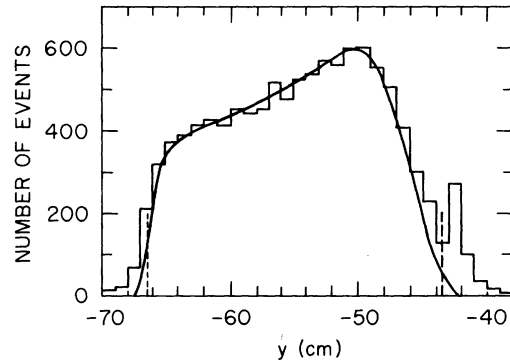


FIG. 8. Distribution of event vertices; projection along y (cm). Smooth curve represents the Monte Carlo prediction. $\chi^2=28$ for 21 degrees of freedom. Dashed lines indicate limits applied in selection of data and in the χ^2 calculation.

of the upstream track which was associated with the shower by the scanner. (61 events were rejected.)

(d) To eliminate events having low detection efficiencies or large momentum measurement errors, both tracks in the upstream gap of the chamber were required to have momenta between 100 MeV/c and 1500 MeV/c. The laboratory momentum spectra for electrons and pions in K_{e3}^0 decay

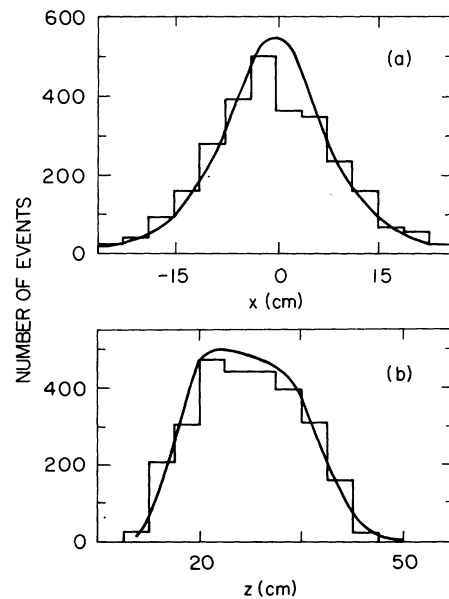


FIG. 9. Distributions of points of traversal on the radiator plane, for the electron in K_{e3}^0 events. (a) projection along x (cm) ($\chi^2=48$ for 11 degrees of freedom) and (b) projection along z (cm) ($\chi^2=19$ for 8 degrees of freedom). Smooth curves represent the Monte Carlo prediction.

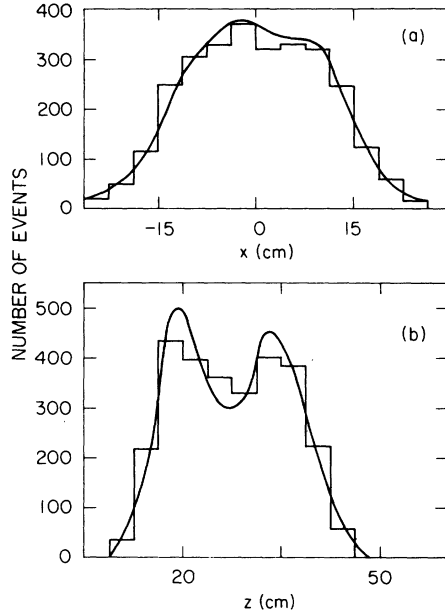


FIG. 10. Distributions of points of traversal on the radiator plane, for the pion in K_{e3}^0 events. (a) projection along x (cm) ($\chi^2=11$ for 11 degrees of freedom) and (b) projection along z (cm) ($\chi^2=16$ for 8 degrees of freedom). Smooth curves represent the Monte Carlo prediction.

are shown in Figs. 11 and 12, respectively. The momentum limit eliminated the long flat tails which characterized these distributions. (288 events were rejected.)

(e) Due to random measurement errors, the zero-constraint kinematic reconstruction could result in nonphysical solutions. In these cases, constrained least-squares fits to select events having acceptable physical solutions were made. The quantity that was minimized was

$$D^2 = (\delta\vec{p}_e, \delta\vec{p}_\pi) G^{-1} (\delta\vec{p}_e, \delta\vec{p}_\pi)^T,$$

where the vector $(\delta\vec{p}_e, \delta\vec{p}_\pi)$ represents the devia-

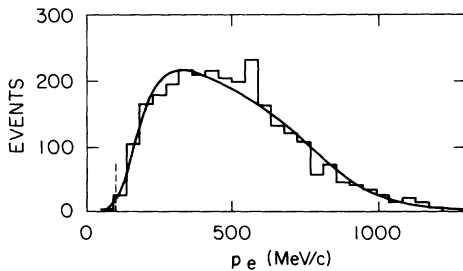


FIG. 11. Laboratory momentum spectrum for electrons in K_{e3}^0 events. Smooth curve represents the Monte Carlo prediction. $\chi^2=36$ for 18 degrees of freedom. Dashed line represents lower limit applied in selection of data and in χ^2 calculation; upper limit at 1500 MeV/c.

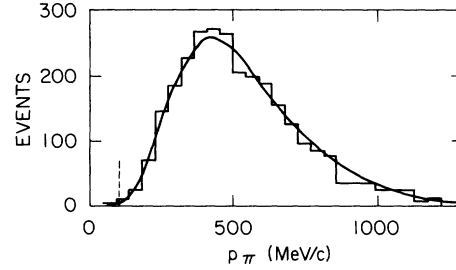


FIG. 12. Laboratory momentum spectrum for pions in K_{e3}^0 events. Smooth curve represents the Monte Carlo prediction. $\chi^2=18$ for 17 degrees of freedom. Dashed line indicates lower limit applied in selection of data and in χ^2 calculation; upper limit at 1500 MeV/c.

tions of the fitted vertex momenta from the measured momenta, and G is the error matrix of the measured momenta referred to the vertex. Improbable events were excluded by requiring that the quantity D^2 be less than 2. (70 events were rejected.)

(f) To eliminate background electron pairs from Dalitz decays of the π^0 from $K_L^0 \rightarrow 3\pi^0$, the invariant mass for both particles, assumed to be electrons, was required to be greater than 70 MeV/c². (20 events were rejected.) The resulting opening-angle distribution for K_{e3}^0 events after applying this restriction is shown in Fig. 13.

(g) The contamination from $K_{\pi 3}^0$ decay can be estimated from the distribution of the quantity $p_0'^2$, which is the square of the K_L^0 momentum in the coordinate system where the two charged particles (assumed to be pions) have zero total longitudinal momentum. $p_0'^2$ may be written as follows¹²:

$$p_0'^2 = \frac{(m_K^2 - m_{\pi^0}^2 - m_c^2)^2 - 4 m_{\pi^0}^2 m_c^2 - 4 m_K^2 p_{ct}^2}{4(p_{ct}^2 + m_c^2)},$$

where m_c is the invariant mass of the charged pion

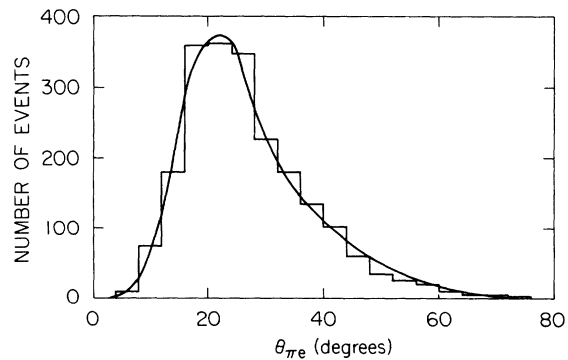


FIG. 13. Laboratory π - e opening angle (degrees) for K_{e3}^0 events. Smooth curve represents the Monte Carlo prediction. $\chi^2=9$ for 10 degrees of freedom.

pair and p_{ct} is their total transverse momentum. For charged $K_{\pi 3}^0$ events, this quantity should be positive. Figures 14(a) and 14(b) show the distributions of this quantity for the K_{e3}^0 and $K_{\pi 3}^0$ candidates, respectively. In order to eliminate $K_{\pi 3}^0$ contamination, $p_0'^2$ for our K_{e3}^0 sample was required to be less than -4000 $(\text{MeV}/c)^2$. This limit together with that used in selecting $K_{\pi 3}^0$ events is indicated in the figures. (202 events were rejected.)

(h) The downstream tracks were extrapolated to the Q -counter plane and required to traverse two or more Q -counter pairs. Due to the uncertainties in the magnetic field in the region of the Q counters,⁵ a one-inch tolerance was allowed on the outside periphery of the Q counters. (989 events were rejected.) Reasons for this rather large number of rejects are (i) particles traversing the Lucite light pipes of the Q counters produced Čerenkov radiation and counted with an estimated efficiency of 30–100%; (ii) the γ rays produced in the electromagnetic shower at the radiator were converted in and detected by the Q counters. Since the efficiencies in detecting events in both cases were not known and could not be compensated for, a strict Q -counter trigger test was applied to tracks in the final selection of events. However, there remains still a possible systematic bias due to the uncertain magnetic field in the region near Q counters, and this will be dealt with in Sec. IV F.

After the rejection of events as described above we are left with a final-event sample of 2171.

III. ANALYSIS AND RESULTS

A. Monte Carlo simulation of K_{e3}^0 decay

In order to correct for the selective trigger and scanning criteria used in this experiment, a Monte Carlo calculation was performed in which a simulated sample of events was generated on a digital computer.

The simulated events were generated at random in the K_L^0 rest frame. A pure vector interaction with a constant form factor was used, for which the distribution density on the pion-electron energy plane (E_π^*, E_e^*) is³

$$\begin{aligned} (dN^2/dE_\pi^* dE_e^*) = & 2E_e^*(m_K - E_\pi^* - E_e^*) \\ & - m_K(E_{\pi \max}^* - E_\pi^*), \end{aligned}$$

where m_K is the K_L^0 rest mass and $E_{\pi \max}^*$ is the maximum pion total energy in the K_L^0 rest frame.

A pair of energies (E_π^*, E_e^*) was picked randomly within the physical region of the Dalitz plot according to this density distribution. The vector momenta of the two particles in the center-of-mass system were calculated. Next the K_L^0 momentum

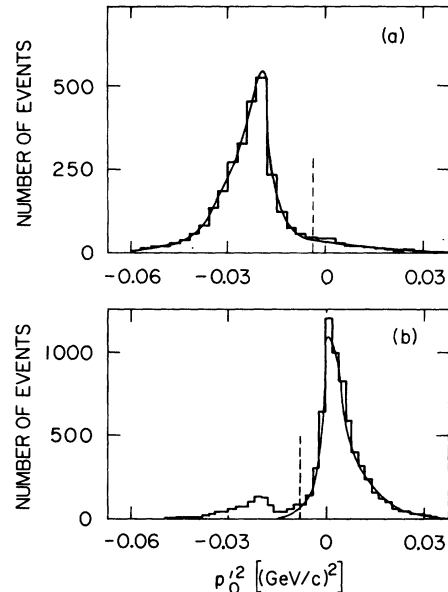


FIG. 14. $p_0'^2$ distribution $(\text{GeV}/c)^2$ (a) for K_{e3}^0 events ($\chi^2=9$ for 12 degrees of freedom) and (b) for $K_{\pi 3}^0$ events ($\chi^2=17$ for 16 degrees of freedom). Dashed lines indicate limits applied in selection of data and in the χ^2 calculation.

was randomly chosen according to a distribution determined experimentally,⁴ and the center-of-mass quantities were transformed to the laboratory. The decay position, or vertex, was then chosen randomly according to the geometry of the target, the collimator system, and the scintillation counters. The particle trajectories downstream from the vertex were calculated with the same computer program that was used to extrapolate real tracks. The trigger criterion at the counter plane (S_1, S_2) (in Fig. 2) was applied and the trajectories were extrapolated to the radiator plane.

The electromagnetic shower of the electron due to the lead radiator of 0.79 radiation length was simulated with a Monte Carlo shower program.^{13,14} The secondary electrons (or positrons) which emerged from the downstream side of the radiator were required to have momenta ≥ 20 MeV/c and an angle with the radiator of $\geq 45^\circ$ in order to assure efficient detection. In general they were required to satisfy the selection criteria used in scanning for K_{e3}^0 decays. The secondary electron(s) passing these tests and the pion (after random multiple scattering and energy loss in the radiator were introduced) were extrapolated to the Q counters to see if the event satisfied all the trigger and scanning criteria. In order to save computation time and reduce fluctuations, the electron-shower simulation and the Q -counter trigger-criterion test were repeated four times for each event. The

fraction of successes was recorded for each event and was used later as a weight factor, W_s .

In this simulation, the following additional effects and corrections were introduced into the Monte Carlo sample in order to be able to refine the comparisons with the experimental sample:

(a) A random measurement error, experimentally determined, and a random small-angle multiple scattering due to the material of the S counters and the vacuum window, were associated with each simulated track at the upstream entry point of the spark chamber.

(b) The K_L^0 direction was also altered to simulate the effect of the uncertainty in the beam direction. In addition, the effects of multiple scattering of K_L^0 mesons in the lead γ -ray absorber and the beam-defining collimator walls were considered. The fraction of events produced by scattered K_L^0 mesons, but still remaining in the sample after fiducial-volume restrictions, was estimated using the tails of the distributions in Figs. 6 and 7. This same fraction of Monte Carlo events was randomly chosen and their K_L^0 directions were altered appropriately.

All events were recalculated with the above effects exactly as were the experimentally measured events. Vertex position and energies in the K_L^0 rest frame were recalculated, using the altered track quantities at the beginning of the chamber. All criteria that were imposed on the selection of the experimental sample were imposed on the Monte Carlo sample and the kinematic reconstruction was also computed by the same program.

(c) Also included in the Monte Carlo sample were 2.2% $K_{\mu 3}^0$ events similarly generated and 2.8% $K_{e 3}^0$ events with the electron and pion interchanged in the kinematic reconstruction. These events which result from pion nuclear interactions in the radiator were introduced to compensate for the inclusion of such events in the experimental sample as discussed in Sec. IV D.

Using this Monte Carlo program and applying the above corrections, the relative detection efficiency for $K_{e 3}^0$ decay was determined. Figure 15(a) shows contours of constant detection efficiency over the Dalitz plot. In Fig. 15(b) the relative efficiency in the kaon center-of-mass system is plotted as a function of q^2 .

B. Determination of the λ_+ parameter

Due to the zero-constraint kinematical fit for each event, two solutions are obtained for the K_L^0 momentum and center-of-mass quantities, e.g., E_π^* . From Monte Carlo comparisons with experimental data, the lower-kaon-momentum solution was found to be the most probable. A comparison

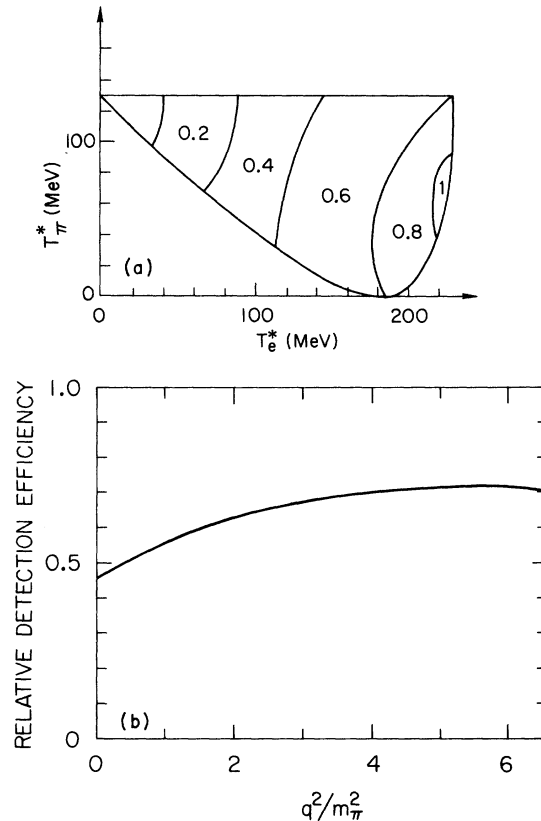


FIG. 15. (a) Relative detection efficiency over (T_π^*, T_e^*) Dalitz plot. (T_π^*, T_e^*) are (pion, electron) kinetic energies in the K_L^0 center-of-mass system. (b) Relative detection efficiency as a function of q^2 .

of the Monte Carlo and experimental distributions for the lower-momentum solution for E_π^* was used to determine the best-fit value for the λ_+ parameter. In this comparison the effective number of Monte Carlo events used was 2.5 times the final selected number of experimental events.

In the Monte Carlo simulation the energy-dependent parameter λ_+ in the form factor was assumed to be zero. Instead of generating further Monte Carlo samples with different assumed values of λ_+ , a weight depending on λ_+ was assigned to each Monte Carlo event according to the following equation:

$$W = W_S W_R \left(1 + \lambda_+ \frac{q^2}{m_\pi^2} \right)^2,$$

where q^2 was calculated using the true rest-frame pion energy E_π^* of the Monte Carlo events. The quantity W_S is the probability that the electron will produce a visible shower which also triggers the Q counters (see Sec. III A), and the quantity W_R is the radiative correction factor, determined from the published results of Ginsberg.¹⁵

The weighted distribution for the lower- K_L^0 momentum solution of the pion energy E_π^* for the Monte Carlo sample was then compared with the distribution of the same quantity for the experimental sample. The weight of each Monte Carlo event was normalized so that the sum of weights was equal to the total number of events in the experimental sample. The λ_+ value was then calculated by determining the minimum value for χ^2 given by the relation

$$\chi^2 = \sum (N_i - (\sum W)_i)^2 / [(\sum W)_i + (\sum W^2)_i],$$

where i is the index of the E_π^* energy interval and, in each interval, N_i is the number of experimental events, $(\sum W)_i$ is the sum of the normalized weights, and $(\sum W^2)_i$ is the sum of the squares of those weights. The χ^2 values calculated were plotted as a function of the λ_+ parameter used in the weighting and is shown in Fig. 16. The best estimate of λ_+ was 0.040 ± 0.010 , where the error is the statistical error only. Possible systematic errors are discussed in Sec. IV. The final result is $\lambda_+ = 0.040 \pm 0.012$.

Using the weights corresponding to the best estimated values of λ_+ , the Monte Carlo distributions were determined for a number of laboratory quantities. These were compared with experimental distributions in Figs. 5–14, where the Monte Carlo distributions have been indicated by solid curves. The χ^2 values for each distribution were evaluated between the indicated limits using the formula appearing above. In performing these calculations, when the number of events per interval was below 50, intervals were summed together.

Figures 5–10 show plots of position distributions in the laboratory. These distributions are not sensitive to different values of λ_+ , but indicate the degree to which the simulation matched the observed

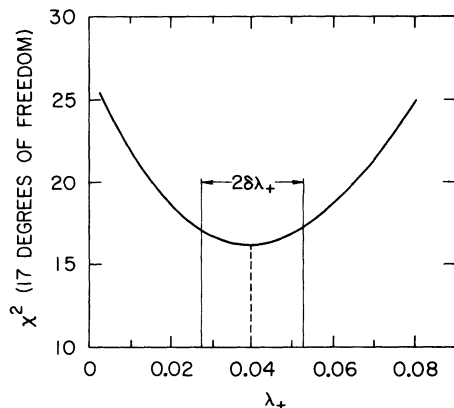


FIG. 16. χ^2 curve to determine λ_+ assuming a form factor $f_+(q^2) = f_+(0)(1 + \lambda_+ q^2/m_\pi^2)$.

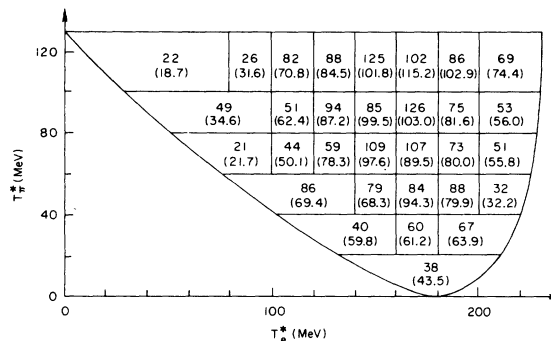


FIG. 17. Experimental distribution of K_{e3}^0 events on (T_π^*, T_e^*) Dalitz plot (low- K_L^0 -momentum solution). (T_π^*, T_e^*) are (pion, electron) kinetic energies in the K_L^0 center-of-mass system. Monte Carlo predictions are shown in parentheses. $\chi^2 = 36.5$ for 31 degrees of freedom.

distributions in the laboratory. Relatively high χ^2 values are noted; however, the general behavior of these experimental distributions is consistent with that predicted by the simulation.

Figures 11, 12, and 13 show plots related to the laboratory vector momenta of secondaries. These quantities are more related to the characteristics of the decay but are still insensitive to the value of λ_+ . Generally good agreement is seen except in Fig. 11 which, due to unexplained peak at $p_\pi = 575$ MeV/c, gave a χ^2 of 36 for 18 degrees of freedom.

The Dalitz plot for the low- K_L^0 -momentum solution is shown in Fig. 17. The experimental results and the Monte Carlo results (with best-fit λ_+) are compared over the 31 regions and they are in good agreement.

Various other phenomenological forms for $f_+(q^2)$ also were fitted using the minimum χ^2 method. For the single-pole form, $f_+(q^2) = f_+(0)(1 - q^2/m^2)^{-1}$, the best-fit value for m was 780_{-80}^{+170} MeV/c². ($\chi^2 = 17$ for 17 degrees of freedom.) For a dipole form, $f_+(q^2) = f_+(0)(1 - q^2/m^2)^{-2}$, the best-fit value for m was 1080_{-130}^{+210} MeV/c². ($\chi^2 = 16.5$ for 17 degrees of freedom.) A quadratic dependence, $f_+(q^2) = f_+(0)(1 + \lambda_+ q^2/m_\pi^2 + \lambda'_+ q^4/m_\pi^4)$, also was fitted to the experimental data, with the resulting best-fit values of $\lambda_+ = 0.050 \pm 0.023$ and $\lambda'_+ = -0.002 \pm 0.005$. ($\chi^2 = 16.2$ for 16 degrees of freedom.) The correlation between λ_+ and λ'_+ was found to be $(d\lambda'_+/d\lambda_+) = -0.2$.

IV. STUDY OF POSSIBLE SYSTEMATIC EFFECTS

In this section a number of systematic effects are considered and the resulting correction to λ_+ , i.e., $\Delta\lambda_+$ is given for each. These corrections were applied in obtaining the final value given here for λ_+ . The uncertainties in these corrections,

i.e., $\delta(\Delta\lambda_+)$ were added in quadrature to the statistical error to give the quoted error value.

A. Random measurement errors

The main source of random errors in the determination of the K -decay position and the particle vector momenta at the vertex was the random error in measurement of points on the film. When the measured laboratory quantities were transformed into the K_L^0 rest frame, the errors became asymmetrical and produced a systematic shift in λ_+ . Had the measurement error of 5μ on the film not been taken into account in the analysis,¹⁶ the best-fit value of λ_+ would have changed by $\Delta\lambda_+ = +0.013$. The uncertainty in the measurement error was $\pm 1 \mu$ and this gives an uncertainty in $\Delta\lambda_+$ of $\delta(\Delta\lambda_+) = \pm 0.002$.

The magnitude of the random error of 5μ was calculated in TVGP. This value was confirmed in special calibration runs made with the central radiator removed, in which measurements on particle tracks in the upstream and downstream gap were compared. The differences were found to agree with that expected from this film-setting error but with an uncertainty of 20%. Additional confirmations came from a study of the reconstructed position of a brass target placed inside the vacuum box in the neutral beam and from the Monte Carlo prediction of the observed distribution for ρ , the distance of closest approach between tracks (shown in Fig. 5).

B. Chamber distortion

A systematic error in the determination of the particle position resulted from the drift of the ionization electrons during the time of spark formation (~ 150 nsec). Studies of film taken with the radiator removed showed that this drift averaged 3.8 mm along \vec{E} and 0.65 mm along $\vec{E} \times \vec{B}$. The average drift was corrected for in the analysis; however, there remained a small nonuniform systematic drift along the track due to the nonuniform magnetic and electric fields. This systematic distortion corresponded to about $\frac{1}{5}$ of that caused by random measurement error and was taken into account in the over-all calibration discussed in Sec. IV C.

C. Over-all calibration for momentum measurements

An over-all correction for the measurement of momentum may be obtained from a study of the invariant mass for K_S^0 mesons, which were coherently regenerated in the special regenerator runs previously mentioned and of the $\pi^+ \pi^-$ invariant mass for the charged pions in $K_{\pi 3}^0$ decay. The re-

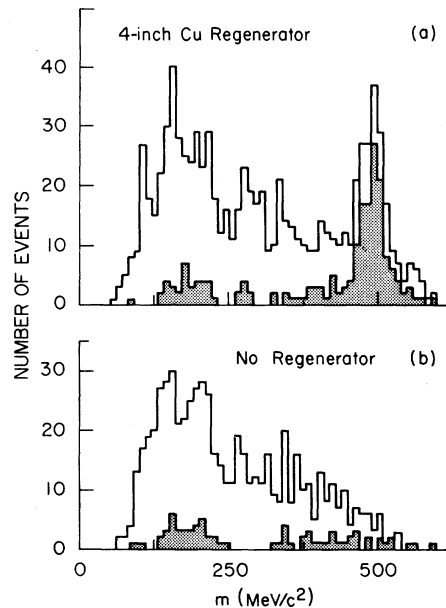


FIG. 18. Histogram for the $\pi^+ \pi^-$ invariant mass for V events, (a) when a 4-in. Cu regenerator was placed 2.25 in. upstream from anticounter A , and (b) with no regenerator. Histogram for events having vector sum of π^+ and π^- momenta within 1.8° of the beam direction shown shaded.

sultant correction took the form of a scale factor for the magnetic field.

Samples of V events were measured for runs with and without a regenerator. Figure 18 shows the invariant mass distributions, assuming the two charged particles were pions. The events included in the shaded histograms were required to have the direction of the vector sum of the momenta of the two charged particles within 1.8° of the K_L^0 beam direction. Events without shower tracks or converted γ 's taken without regenerator were used to determine the three-body-decay background. The regenerator run with the background subtracted showed a single peak at 496.3 MeV/ c^2 with a spread of the ± 16.4 MeV/ c^2 and an average value of 496.3 ± 2.0 MeV/ c . This result, based on the analysis of 2000 V events, did not determine the magnetic-field scale factor as precisely as was required. Rather than increase the statistical sample it was decided to employ the method described below.

The distribution of invariant mass of the charged pions in $K_{\pi 3}^0$ decay is also sensitive to this scale factor for the magnetic field. Comparing the Monte Carlo generated distribution of this invariant mass with the experimental distribution calculated for varying magnetic fields, a best-fit distribution was searched for. The χ^2 showed a minimum at a χ^2 value of 14.0 for 18 degrees of free-

dom. The scale factor at the χ^2 minimum deviated from unity by $(0.55 \pm 0.13\%)$. This result agreed in magnitude and sign with that from the K_S^0 invariant mass study and was used in the analysis of the data. The uncertainty in this correction results in an uncertainty in λ_+ of $|\delta(\Delta\lambda_+)| \leq 0.002$.

D. Contaminations in the experimental sample

In the scanning criteria for the selection of K_{e3}^0 events in this experiment, no distinction was made between possible pion nuclear interactions in the radiator and electron showers. Thus the selected sample contained some $K_{\pi 3}^0$ and $K_{\mu 3}^0$ events. There were also some K_{e3}^0 events with the pion misidentified as an electron.

From the $p_0'^2$ distribution of Fig. 14(a), the discrepancy between the Monte Carlo simulation and the experiment in the positive $p_0'^2$ region indicated that there were about $48 \pm 10 K_{\pi 3}^0$ events or 2.3% of the experimental sample. These $K_{\pi 3}^0$ events were virtually eliminated from the final K_{e3}^0 sample by the exclusion of events with $p_0'^2$ larger than -4000 $(\text{MeV}/c)^2$, i.e., criterion (g) of Sec. II E.

The number of $K_{\mu 3}^0$ events and of K_{e3}^0 events with the pion misidentified as an electron cannot be estimated directly. However, since the laboratory pion momentum distribution of these decay modes was similar to that of the $K_{\pi 3}^0$ mode, the probability of a pion interaction in these decay modes should also be the same. Using the known branching ratios of the decay modes and their trigger efficiencies, it was estimated that there were about $48 \pm 10 K_{\mu 3}^0$ events appearing as K_{e3}^0 events and $59 \pm 12 K_{e3}^0$ events with pions misidentified as electrons. Consequently, these events were not eliminated, but their effect was corrected for by introducing the same contaminations in the Monte Carlo sample. The change in λ_+ due to the inclusion of these events was $\Delta\lambda_+ = -0.009$, with an uncertainty of $\delta(\Delta\lambda_+) = \pm 0.003$.

Another possible source of contamination was electron pairs (Dalitz pairs) from decaying π^0 in $K_L^0 \rightarrow 3\pi^0$. These events were essentially eliminated by the selection criterion (f) in Sec. II E. Contamination from other modes of decay was negligible.

E. K_L^0 beam parameters

In the zero-constraint kinematic reconstruction of neutral three-body decay, precise knowledge of the beam direction is very important. In this experiment, the K_L^0 beam direction was determined to ± 0.8 mrad from a study of regenerated K_S^0 events. The spread in the beam direction due to scattering of the beam in the lead γ -ray absorber and the beam-defining collimator walls was also

considered and compensated for by introducing the same amount of spread in the Monte Carlo simulation. [See Sec. III A(b).] The effect on λ_+ from introducing this beam spread into the Monte Carlo analysis was $\Delta\lambda_+ = -0.008 \pm 0.002$.

The K_L^0 momentum spectrum was determined in the study reported previously and was also confirmed in this K_{e3}^0 analysis.⁴ The uncertainty in it was small and the effect on the error in λ_+ was $\delta(\Delta\lambda_+) < 0.001$.

F. Uncertainty in the trigger condition

The magnetic field in the Q-counter region was not mapped,⁵ but was extrapolated from the mapped region using Maxwell's equations. The extrapolation of tracks in this region was subject to systematic shifts of up to $\pm \frac{1}{8}$ in. Due to the considerations discussed in (h) of Sec. II E, it was necessary to extrapolate all tracks to this region to verify the trigger condition. The uncertainty in the position of tracks at the Q-counter plane gives an uncertainty in the trigger efficiency which, in turn, could bias the value of λ_+ . This bias was only partially compensated for by using the same extrapolated magnetic field to extrapolate real and simulated tracks and by allowing a one-inch tolerance around the Q counters for the position of real tracks. The resulting uncertainty in λ_+ due to this effect was estimated to be $\delta(\Delta\lambda_+) = \pm 0.003$.

G. Other small systematic effects

The scanning inefficiency was $\sim 4\%$ as determined from the rescanning of one third of the film. The effect on λ_+ of the inclusion of the events found in the rescanning was small and was estimated not to exceed $\delta(\Delta\lambda_+) = \pm 0.001$.

The radiative correction was introduced in the analysis. Without this correction, the value of λ_+ estimated would have increased by $\Delta\lambda_+ = 0.002$. Since this correction is very small, the uncertainty in the correction should be even smaller and was ignored.

From the laboratory pion spectrum of the K_{e3}^0 sample, it was estimated that 1% of the pions decayed into muons before they traversed the upstream gap of the wide-gap chamber, where the momentum was measured. Those with decay muon momentum or direction, sufficiently different from that of the pion, were eliminated either in the geometric reconstruction program TVGP or by the resulting large distance of closest approach between the pion and electron tracks at the vertex. The effect of those events still remaining in the sample was small and any bias introduced into the sample was negligible when transformed in the kaon rest frame.

A summary of corrected systematic errors, $\Delta\lambda_+$, and the estimated contribution to the error in λ_+ after their correction, $\delta(\Delta\lambda_+)$, is given in Table I.

V. DISCUSSION AND CONCLUSION

The result obtained in this experiment for λ_+ in K_{e3}^0 decay is 0.040 ± 0.012 . The error includes the effect of the uncertainties in the correction for systematic errors, i.e., $\delta(\Delta\lambda_+)$, which were discussed in Sec. IV. These errors were added in quadrature to the statistical error to obtain the quoted error. The correlation between these systematic errors was not investigated. Were the systematic errors assumed to be strongly correlated, the values for $\delta(\Delta\lambda_+)$ should be added linearly and then quadratically combined with the statistical error. The result assuming this most unfavorable case would be $\lambda_+ = 0.040 \pm 0.017$.

The λ_+ value obtained is in poor agreement with theoretical predictions of ~ 0.023 and with many K_{e3}^0 experimental results.³ A summary of recent experimental measurements¹⁷⁻²⁶ for λ_+ and an average value for earlier measurements are given in Table II. The consistency between these results is indeed poor indicating only that λ_+ should lie in the range of 0.03 to 0.06. In the analysis of this experiment, a rather large sensitivity to what might normally be considered small systematic effects was observed. It would seem that the large discrepancies in the results for λ_+ (and λ'_+) obtained in a number of even recent experiments could be due, in part, to such systematic effects.

The recent analysis of K_{e3} made by Chounet *et al.*²⁷ selected out some of the more precise determinations of the form factor in K_{e3}^0 and K_{e3}^+ decay and obtained a combined best-fit value for both linear and quadratic forms for the form factor. The value for the linear form was $\lambda_+ = 0.038 \pm 0.002$. ($\chi^2 = 79$ for 51 degrees of freedom.) For a fit using the quadratic form they obtained $\lambda_+ = 0.012 \pm 0.005$ and $\lambda'_+ = 0.0052 \pm 0.0013$ with an improved χ^2 of 63 for 51 degrees of freedom. The results reported

TABLE I. Summary of systematic errors, $\Delta\lambda_+$, and remaining errors after correction, $\delta(\Delta\lambda_+)$.

Effect	$\Delta\lambda_+$	$\delta(\Delta\lambda_+)$
Random measurement error (A)	+0.013	± 0.002
Chamber distortion (B)	+0.002	...
Momentum calibration (C)	...	<0.002
Contamination of sample (D)	-0.009	± 0.003
K_L^0 beam parameters (E)	-0.008	± 0.002
Uncertain trigger condition (F)	...	± 0.003
Scanning inefficiency (G)	...	<0.001
Radiation correction (G)	+0.002	...

TABLE II. Summary of experimental results on λ_+ .

		λ_+
Average values from earlier experiments (Ref. 3)		
K_{e3}^0		0.017 ± 0.007
K_{e3}^+		0.030 ± 0.007
		(0.045) ^a
$K_{\mu 3}^+$		0.045 ± 0.012
Recent experimental results		
K_{e3}^0	C. Y. Chien <i>et al.</i> ^{17,18}	0.05 ± 0.010
K_{e3}^0	V. Bisi <i>et al.</i> ¹⁹	0.023 ± 0.005
K_{e3}^0	G. Neuhofer <i>et al.</i> ²⁰	0.022 ± 0.014
K_{e3}^+	H. J. Steiner <i>et al.</i> ²¹	0.027 ± 0.010
K_{e3}^+	I-H. Chiang <i>et al.</i> ²²	0.029 ± 0.011
$K_{\mu 3}^0$	C. Y. Chien <i>et al.</i> ²³	0.08 ± 0.010
$K_{\mu 3}^0$	M. G. Albrow <i>et al.</i> ²⁴	0.085 ± 0.015
$K_{\mu 3}^+$	D. Haidt <i>et al.</i> ²⁵	0.060 ± 0.019
$K_{\mu 3}^+$	C. Ankenbrandt <i>et al.</i> ²⁶	0.024 ± 0.022
K_{e3}^0	This experiment	0.040 ± 0.012

^a This value could not be excluded. See Ref. 3.

here are in good agreement with the linear-form fit of Chounet *et al.* The quadratic-form fit to our data gives a value for λ'_+ consistent with zero. (See Sec. IIIB.) The determination of the q^2 dependence for the form factor indeed requires further experimental investigation.

ACKNOWLEDGMENTS

We would like to thank the staff of the Brookhaven AGS and, in particular, T. Blair, J. Tanguay, and J. Desmond for their cooperation and aid during the preparation and running of this experiment.

We are grateful to Professor G. A. Snow, Professor T. B. Day, and Professor S. Oneda for many helpful discussions, and to Professor R. G. Glasser and Professor P. H. Steinberg also for their contributions to the analysis.

The assistance of W. E. Crowe, R. E. Hummer, S. A. Killion, M. L. Kreithen, P. E. Goldhagen, and A. McDonald in the designing, constructing, and maintaining of much of the equipment is gratefully acknowledged. We also thank M. E. Talbert, P. A. Warden, D. B. Twitty, and a large group of student scanners and measurers for their aid in the scanning and the analysis of the film.

*Work supported in part by the U. S. Atomic Energy Commission.

†Present address: Stanford Linear Accelerator Center, Stanford, California 94305.

‡Present address: Westinghouse Research Laboratory, Pittsburgh, Pennsylvania 15235.

§Present address: Washington University, St. Louis, Missouri 63130.

||Deceased.

¹See, for example, N. Cabibbo, in *Particle Symmetries and Axiomatic Field Theory*, 1965 Brandeis Summer Institute in Theoretical Physics, edited by M. Chrétien and S. Deser (Gordon and Breach, New York, 1966), Vol. 1, pp. 1-96.

²R. E. Marshak, Riazuddin, and C. P. Ryan, *Theory of Weak Interactions in Particle Physics* (Wiley, New York, 1969).

³M. K. Gaillard and L. M. Chounet, CERN Report No. CERN 70-14, 1970 (unpublished).

⁴The K_L^0 momentum distribution observed at the chamber was assumed to be of the form

$$dN_K/dp_K \propto (p_K^{-1} e^{-0.67/p_K}) (e^{Ap_K - Bp_K^2}),$$

where p_K is the K_L^0 momentum and where the last term in parenthesis is the distribution at production. The experimentally determined values for A and B were $A = 0.540 \pm 0.016$ (GeV/c)⁻¹ and $B = 0.669 \pm 0.380$ (GeV/c)⁻². (See Ref. 6.)

⁵Hall-probe measurements were made in 1 in. \times 3 in. \times 4 in. intervals throughout most of the useful volume. (Measurements were not extended to include the whole area of the Q-counter plane.) Fourth-order polynomials were fitted in 57 overlapping subdivisions of the field. In each region the coefficients for the polynomials were constrained by Maxwell's equations. The probe and the associated electronics were furnished by the Brookhaven 30-in. Hydrogen-Bubble-Chamber Group. Their Cooperation and advice in making these measurements are gratefully acknowledged.

⁶R. C. Smith, L. Wang, M. C. Whatley, G. T. Zorn, and J. Hornbostel, Phys. Lett. **32B**, 133 (1970); R. C. Smith, L. Wang, M. C. Whatley, and G. T. Zorn, University of Maryland Technical Report No. 70-105, 1970 (unpublished); R. C. Smith, Ph.D. thesis, University of Maryland, 1970 (unpublished).

⁷L. Wang, R. C. Smith, M. C. Whatley, and G. T. Zorn, *International Symposium on Nuclear Electronics, Versailles, France, 10-13 September 1968* (Société Française des Electroniciens et des Radioelectriciens, Versailles, France, 1968), Vol. 3.

⁸The reason for this large brightness variation, which occurred even for tracks in the same photograph, is thought to have been due principally to the low pulsed-voltage requirement which was necessary to prevent sparking around the outside of the chamber and the resulting long spark-formation time (~ 150 nsec).

⁹The two-view film projectors were designed for 35-mm single-frame or double-frame film advance. The lenses used were 51-mm $f/4$ Componon lenses manufactured by Schneider-Kreuznach. The film was clamped between two $\frac{1}{4}$ -in. thick glass plates. The $\frac{1}{4}$ -in. glass on the lens side also caused barrel distortion, which dominated over the pincushion distortion of the lenses. The least count of the image-plane digitizer was 25 μ . The digitizer and measuring tables

were manufactured by Wayne-George Corporation of Newton, Massachusetts.

¹⁰F. T. Solmitz, A. D. Johnson, and T. B. Day, LRL Alvarez Group Programmers Note No. P-117, 1966 (unpublished); T. B. Day, University of Maryland Technical Report No. 649, 1966 (unpublished).

¹¹G. Wolsky, "FIDCON," University of Maryland Technical Report No. 679, 1967 (unpublished). Using measurements on calibration grids, photographed in place of the spark chamber, this program searched out the best-fit values for the fiducial positions and other optical parameters required for track reconstruction.

¹²D. Luers, I. S. Mitra, W. J. Willis, and S. S. Yamamoto, Phys. Rev. **133**, B1276 (1964).

¹³The shower Monte Carlo program was a modified version of a Fortran program written by M. G. Hauser; bremsstrahlung, pair production, Compton effect, and ionization loss were included. In the modified version that was used, angular deviations in Compton effect and Molière scattering were included and the charge states of the secondaries were identified.

¹⁴L. Wang, Ph.D. thesis, University of Maryland, 1971 (unpublished), and University of Maryland Technical Report No. 73-033, 1973 (unpublished).

¹⁵E. S. Ginsberg, Phys. Rev. **171**, 1675 (1968); *ibid.* **174**, 2169 (1968). W_R was taken to be (1 + the corrected values of Fig. 4).

¹⁶The smallest value of the effective error which was attained by any measurer was 2.5 μ . A more detailed discussion of these errors appears in Ref. 6.

¹⁷C. Y. Chien, B. Cox, L. Ettlinger, L. Resvanis, R. A. Zdanis, E. Dally, P. Innocenti, E. Seppi, C. D. Buchanan, D. K. Drickey, F. D. Rudnick, P. F. Shepard, D. H. Stork, and H. K. Ticho, Phys. Lett. **35B**, 261 (1971).

¹⁸E. Dally, P. Innocenti, E. Seppi, C. Y. Chien, B. Cox, L. Ettlinger, L. Resvanis, R. A. Zdanis, C. D. Buchanan, D. J. Drickey, P. F. Shepard, D. H. Stork, and H. K. Ticho, Phys. Lett. **41B**, 647 (1972).

¹⁹V. Bisi, P. Darriulat, M. I. Ferrero, C. Grosso-Pilcher, K. Kleinknecht, C. Rubbia, A. Staude, and K. Tittel, Phys. Lett. **36B**, 533 (1971).

²⁰G. Neuhöfer, F. Niebergall, M. Regler, H. E. Stier, K. Winter, J. J. Aubert, X. De Bouard, V. Lepeltier, L. Massonnet, H. Pessard, N. Vivargent, T. R. Willits, M. Yvert, W. Bartl, and M. Steuer, Phys. Lett. **41B**, 642 (1972).

²¹H. J. Steiner, S. Natali, F. Romano, D. C. Cundy, J. Lemonne, T. I. Pedersen, P. Renton, L. Behr, V. Brisson, L. Kluberg, P. Petiau, B. Aubert, J. P. Lowys, J. J. M. Timmermans, H. Huzita, F. Mattioli, A. Sconza, D. Gamba, and A. Marzari-Chiesa, Phys. Lett. **36B**, 521 (1971).

²²I.-H. Chiang, M. L. Rosen, S. Shapiro, R. Handler, S. Olsen, and L. Pondrom, Phys. Rev. D **6**, 1254 (1972).

²³C. Y. Chien, B. Cox, L. Ettlinger, L. Resvanis, R. A. Zdanis, E. Dally, P. Innocenti, E. Seppi, C. D. Buchanan, D. J. Drickey, F. D. Rudnick, P. F. Shepard, D. H. Stork, and H. K. Ticho, Phys. Lett. **38B**, 627 (1970).

²⁴M. G. Albrow, D. Aston, D. P. Barber, L. Bird, R. J. Ellison, C. H. Halliwell, R. E. H. Jones, A. D. Kanaris, F. K. Loebinger, P. G. Murphy, M. G. Strong, J. Walters, D. D. Yovanovich, and R. F. Templeman,

Nucl. Phys. **B44**, 1 (1972).

²⁵D. Haidt, J. Stein, S. Natali, G. Piscitelli, F. Romano, E. Fett, J. Lemonne, T. I. Pedersen, S. N. Tovey, V. Brisson, P. Petiau, C. D. Esvelt, J. J. M. Timmermans, B. Aubert, L. M. Chounet, Le Dong, F. Bobisut, H. Huzita, F. Sconza, A. Marzari-Chiesa, and A. E. Werbrouch, Phys. Rev. D **3**, 10 (1971).

²⁶C. Ankenbrandt, R. Larsen, L. Leipuner, L. Smith, F. Shively, R. Stefanski, R. Adair, H. Kasha, S. Merlan, R. Turner, and P. Wanderer, Phys. Rev. Lett. **28**, 1472 (1972).

²⁷L. M. Chounet, J. M. Gaillard, and M. K. Gaillard, Phys. Rep. **4C**, 200 (1972).

PHYSICAL REVIEW D

VOLUME 9, NUMBER 3

1 FEBRUARY 1974

Large-angle elastic proton-proton polarization at 5.15 GeV/c†

G. W. Abshire, C. M. Ankenbrandt,* R. R. Crittenden, R. M. Heinz,
K. Hinotani,‡ S. I. Levy, H. A. Neal,§ and D. R. Rust
Department of Physics, Indiana University, Bloomington, Indiana 47401
(Received 12 August 1973)

We present herein the initial results of a large-angle elastic p - p polarization experiment which is now in progress at the Argonne ZGS (Zero-Gradient Synchrotron) accelerator. Data for the incident proton momentum of 5.15 GeV/c are presented for $30^\circ \lesssim \theta_{c.m.} \lesssim 90^\circ$. These results, which extend to $t \approx -4.0$ (GeV/c)², represent the first high-statistics p - p polarization measurements for $|t|$ values greater than ~ 2.5 (GeV/c)². We observe a minimum in the polarization near $t = -0.8$ (GeV/c)², a smooth increase in the polarization until a maximum is attained near $t = -1.8$ (GeV/c)², and then a monotonic decline in the polarization until the value of zero is reached at $\theta_{c.m.} = 90^\circ$. The data are analyzed in terms of an optical model.

We present here the 5.15-GeV/c results of an experiment presently in progress at the Argonne ZGS to study the polarization in elastic proton-proton scattering at large momentum transfers. A dramatic extension in the t range for high-statistics polarization data has been achieved by utilizing, for the first time at high energies, a polarized-proton target in an external proton beam. At 5.15 GeV/c, data were taken at center-of-mass angles between 30° and 90° , corresponding to the t range $0.5 < |t| < 4.0$ (GeV/c)². The typical statistical error in the polarization is ± 0.03 .

The layout of the experimental apparatus is shown in Fig. 1. A beam of 10^9 - 10^{10} protons per pulse was incident on a 2-inch-long ethylene glycol polarized-proton target. The angular divergence of the incident beam was $\lesssim 2$ mrad. Each of the elastically scattered protons was detected in a multiwire proportional chamber spectrometer whose angular position was remotely controlled. The apparent scattering angle of each scattered proton was determined with a resolution of ± 2.0 mrad, the momentum of each final-state particle was determined with a resolution of $\pm 5\%$, and the difference in the particle transit time to counters FC5 and SC5 was measured with a resolution of ± 0.7 nsec. Thus, in the analysis of each event we could examine the mass of each final-state particle,

the correlation between the two final-state momenta, and the correlation between the two scattering angles. The trigger system itself, consisting of a fourfold coincidence in each arm, defined a laboratory solid angle acceptance of $\lesssim 0.5$ msr for each arm and a time resolution of 10 nsec between the fast-arm and slow-arm coincidences.

The incident beam employed in the experiment was formed by utilizing two septum magnets to split off a small fraction of the ZGS External Proton Beam I. This beam was transmitted through a dispersive optics system to the polarized-proton target (PPT). The gross intensity of the beam was monitored by two ionization chambers in the beam. We employed five separate monitors to determine the relative beam flux incident on the actual polarized-proton target. One monitor (BM) is a scintillator placed in that portion of the beam that illuminates the polarized-proton target. This scintillator is viewed by a photomultiplier whose output is integrated and then digitized. Monitor LM is a three-element telescope which detects particles scattered from a piece of plastic placed in the portion of the beam which illuminates the target. Monitor RM is a three-element telescope which views the polarized-proton target at a large angle. By conducting a highly controlled series of measurements, we have demonstrated that the number

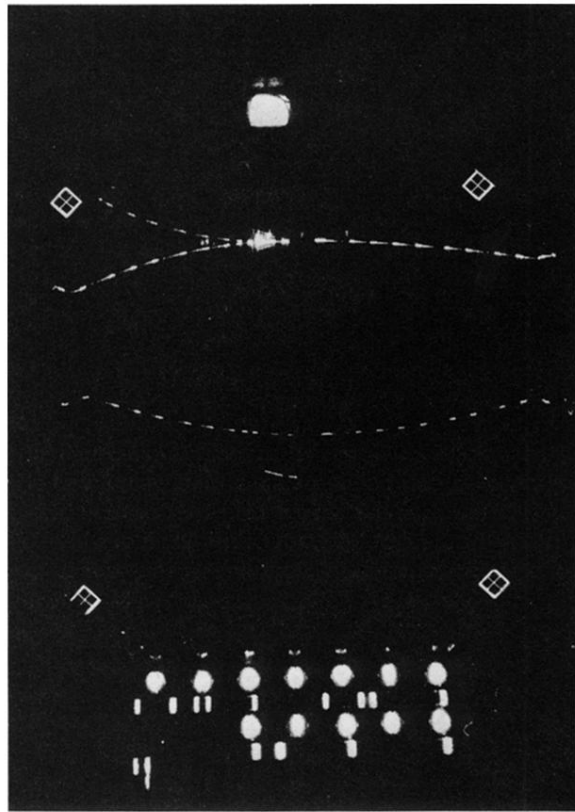


FIG. 3. Photograph of K_{e3}^0 decay.